



OPEN ACCESS

EDITED BY

Manoj Khandelwal,
Federation University Australia, Australia

REVIEWED BY

Bing Bai,
Beijing Jiaotong University, China
Zarghaam Rizvi,
GeoAnalysis Engineering GmbH, Germany

*CORRESPONDENCE

Wenkai Feng,
✉ fengwenkai@cdu.cn

RECEIVED 18 February 2025

ACCEPTED 31 March 2025

PUBLISHED 10 April 2025

CITATION

Lan B, Jia B, Wu Y, Yi X, Feng W and Li Y (2025)
Strength characteristics in saturation process
and rainfall-induced landslide failure
mechanism of granite residual soil.
Front. Earth Sci. 13:1578923.
doi: 10.3389/feart.2025.1578923

COPYRIGHT

© 2025 Lan, Jia, Wu, Yi, Feng and Li. This is an open-access article distributed under the terms of the [Creative Commons Attribution License \(CC BY\)](https://creativecommons.org/licenses/by/4.0/). The use, distribution or reproduction in other forums is permitted, provided the original author(s) and the copyright owner(s) are credited and that the original publication in this journal is cited, in accordance with accepted academic practice. No use, distribution or reproduction is permitted which does not comply with these terms.

Strength characteristics in saturation process and rainfall-induced landslide failure mechanism of granite residual soil

Bing Lan¹, Bangzhong Jia¹, Yiyong Wu^{1,2}, Xiaoyu Yi³,
Wenkai Feng^{3*} and Yihe Li³

¹The Geological Disaster Prevention and Control Technical Center of Guangdong Province, Guangdong Geological Bureau, Guangzhou, China, ²Key Laboratory of Geohazard Prevention of Hilly Mountains, Ministry of Natural Resources of China, Fuzhou, China, ³State Key Laboratory of Geohazard Prevention and Geoenvironment Protection, Chengdu University of Technology, Chengdu, China

The southeastern coastal areas of China have a wide distribution of granite residual soil, and the region experiences heavy rainfall, particularly during typhoons and other climatic events, leading to frequent landslides in the residual layer. This study investigates the hydro-mechanical behavior of Mingqing County (Fujian Province) granite residual soils through direct shear tests and novel meso-structural analysis using scanning electron microscopy (SEM). By systematically evaluating unsaturated, saturated, and continuously saturated states, we quantify the soil's strength deterioration mechanisms and establish, for the first time, a microstructure-based framework linking saturation-dependent structural evolution to macroscopic shear behavior. Results reveal that shear strength declines nonlinearly with increasing moisture content and saturation duration: cohesion follows a quadratic function, while the internal friction angle adheres to a logarithmic relationship. SEM imaging uncovers critical meso-scale processes, including the dissolution of clay-humic cementation and the collapse of metastable pore structures under prolonged saturation, which directly drive strength reduction. During continuous saturation, stress-strain curves exhibit strain-hardening behavior accompanied by distinct stick-slip phenomena post-shear, reflecting progressive particle rearrangement and intergranular bond degradation. Both cohesion and internal friction angle decrease asymptotically until stabilization, governed by saturation-induced microstructural homogenization. These findings provide a scientific basis for further understanding and predicting the disaster mechanisms and failure modes of granite residual soils under heavy rainfall conditions.

KEYWORDS

granite residual soil, saturation time, strength characteristics, mesoscopic structure, failure mechanism

1 Introduction

The southeastern coastal areas of China were significantly impacted by early tectonics, leading to the wide distribution of granite strata across various periods (Zhai et al., 2016; Zhan et al., 2018; Zhao et al., 2019). This granite distribution is concentrated primarily in Guangdong and Fujian provinces, comprising approximately 30%–40% of the area (Cui et al., 2007). The region experiences frequent typhoon occurrences from May to October each year due to its land-ocean climate (Huang et al., 2019; Yang et al., 2020; Wu and Lin, 2021). These typhoons bring heavy rainfall and even extreme rainstorms, leading to the prevalent occurrence of large-scale group shallow landslides in granite areas. Over the 10-year period from 2012 to 2021, the southeastern coastal provinces experienced numerous rainfall-type landslide disasters. Notably, in both 2016 and 2021, typhoons *Niebert* and *Lubi* successively made landfall, triggering heavy rainfall and severely impacting Minqing County, Fujian Province. This unfortunate event resulted in 73 deaths and 17 people reported missing (Bai et al., 2022). In July 2019, Longchuan County, Guangdong Province, experienced four consecutive days of heavy rainfall, with a total accumulation exceeding 260 mm. This intense weather event led to landslides of varying severity in 352 villages across 24 townships within the county (Bai et al., 2021; Feng et al., 2022). Despite the small scale of these landslides, they exhibit typical fluidization characteristics, leading to a considerable expansion of the accumulation range. This results in significant siltation of buildings and cultivated land in the affected area, significantly complicating rescue and post-disaster management efforts (Bai et al., 2021; Li X. et al., 2020).

Residual soil is formed from granite due to long-term physical and chemical weathering. Its mineral composition is abundant in secondary clay minerals, namely, kaolinite and illite, which exhibit strong hydrophilic properties. Additionally, the soil comprises quartz and feldspar with high weathering resistance (Li C. S. et al., 2020; Wang et al., 2021). The unique structural characteristics of granite residual soil render it highly sensitive to water, resulting in significant changes in its mechanical properties. During heavy rainfall, the rapid increase in moisture content frequently leads to a decay in soil strength, subsequently causing a pronounced disintegration phenomenon (Zhang and Tang, 2013; Liu et al., 2019; Wei et al., 2019; Luo et al., 2021; Xia et al., 2022; An et al., 2023; An et al., 2020). Residual soil is a three-phase complex, and its mechanical strength characteristics are determined by the changes in the me-so-structure under external loads during the saturation process (Gao et al., 2020; Zhou, 2020; Yin et al., 2022). Numerous studies have explored the correlation between pore distribution and strength characteristics of structural soils. These studies typically employ a combination of strength mechanics tests and microstructure tests, including scanning electron microscopy (SEM) and mercury intrusion porosimetry (MIP). For example, Griffiths and Joshi (1989) examined the impact of structural differences on clay strength using scanning electron microscopy (SEM) to analyze pore distribution. Zhang et al. (2012) conducted SEM and MIP tests to analyze the evolution of microstructure in Zhanjiang structural clay during the deformation process. They observed three stages of microstructure evolution: structural fine-tuning, structural failure, and structural solidification. Currently,

there is a scarcity of studies on the me-so-structural changes in granite residual soil due to heavy rainfall and external loads. Moreover, the analysis of the resulting strength changes from such meso-structural variations remains inadequate. In granite residual layer landslides triggered by heavy rainfall, rainfall plays a pivotal role. The soil, affected by rainfall, transitions rapidly from an unsaturated to saturated state and eventually reaches a continuously saturated state. During the process of soil saturation, the continuous action of pore water leads to regular changes in the meso-structure of the soil. These changes, in turn, contribute to the deterioration of mechanical strength and ultimately result in a decrease in slope stability, providing in-sights into the rainfall-induced instability mechanism of granite residual layer slopes (Wei et al., 2020; Miao et al., 2022; Pan et al., 2020; Hu et al., 2020).

During heavy rainfall, the granite residual soil undergoes the entire process of unsaturation, saturation, and persistent saturation. Landslide events typically exhibit a hysteresis relative to rainfall (Bai et al., 2022), mainly occurring during the persistent saturation stage of the soil. Further research is required to explore the interplay between meso-structure, mechanical strength, and macro-slope stability throughout the entire saturation process. Particular attention should be given to the soil structure and mechanical properties during the persistent saturation stage. This paper innovatively reveals the changes in mechanical strength of granite residual soils during unsaturated, saturated, and continuously saturated processes, explicitly establishing the quadratic function relationship between cohesion and moisture content, as well as the logarithmic function relationship between internal friction angle and moisture content. Through scanning electron microscopy (SEM), the study analyzes the evolution of the soil's microstructure, providing a micro-mechanical explanation for the observed strength deterioration. Additionally, by combining actual case studies, the research proposes the disaster mechanisms and failure modes of granite residual soil landslides under heavy rainfall conditions.

This study hypothesizes that the strength deterioration of granite residual soils under heavy rainfall is driven by saturation-induced meso-structural degradation, which follows distinct mathematical trends across different saturation phases. To test this hypothesis, we integrate direct shear tests with SEM-based meso-structural analysis to systematically investigate the soil's hydro-mechanical behavior under unsaturated, saturated, and continuously saturated conditions. Our work innovatively establishes quantitative models (quadratic and logarithmic functions) linking moisture content to cohesion and internal friction angle, respectively, while revealing microscale mechanisms underlying strength loss. By bridging meso-structural dynamics to macro-scale shear behavior, this research provides a novel framework for predicting rainfall-induced landslide initiation and evolution, directly informing slope risk management strategies in southeastern China's coastal areas.

2 Materials

2.1 Physical properties of soil

Minqing County, an important county of Fujian Province, located in the southeastern coastal region of China (Figure 1). The granite residual soil samples used in the experiment were

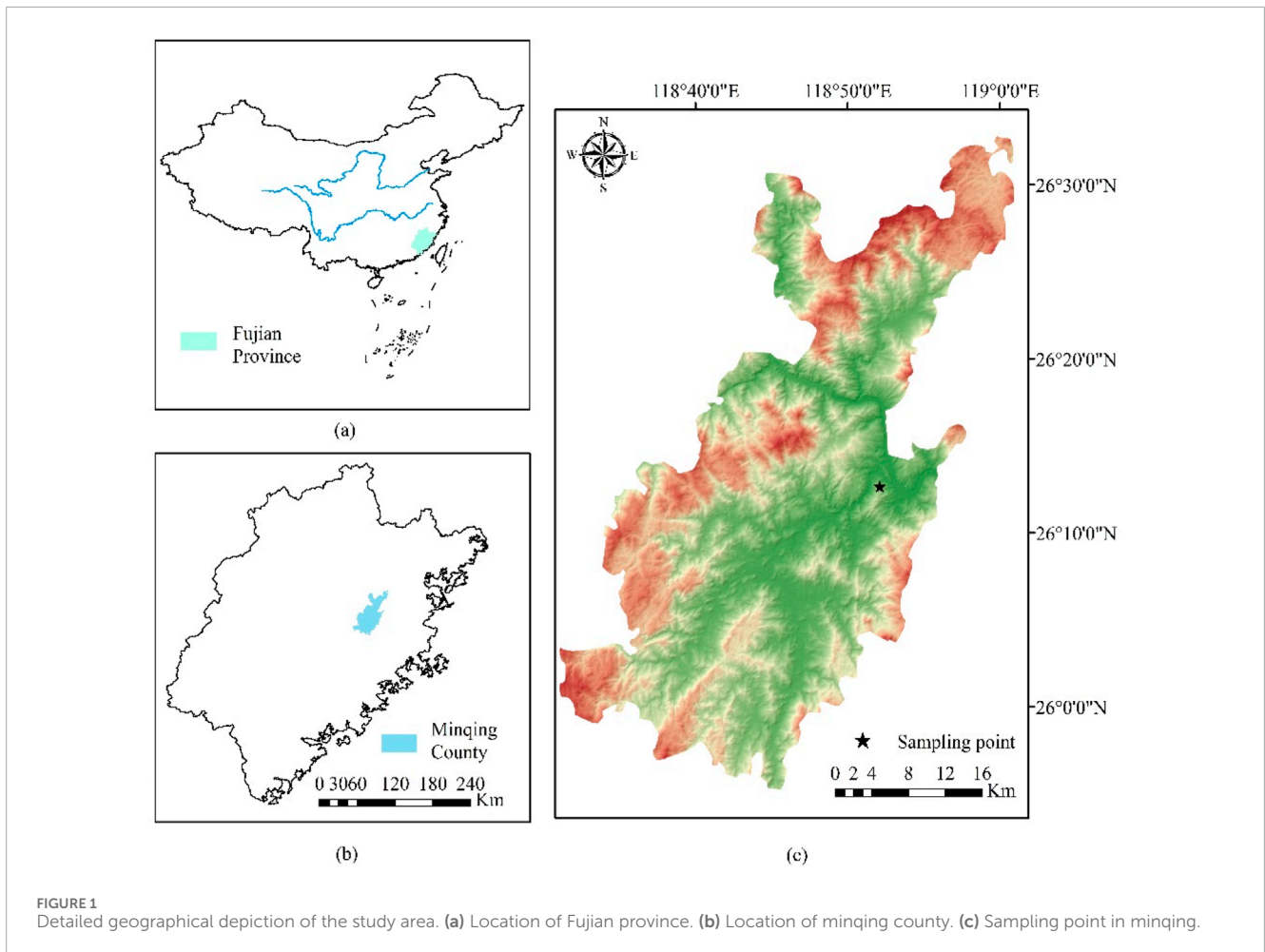


FIGURE 1
Detailed geographical depiction of the study area. (a) Location of Fujian province. (b) Location of minqing county. (c) Sampling point in minqing.

all taken from Minqing County, the granite strata belongs to the late Yanshanian acid neutral intrusive rock, and the lithology is mainly biotite monzonite and quartz diorite. Under the action of perennial weathering, weathering residual layers are generally formed on the surface of granite slopes, which is reddish-brown, and the weathering thickness ranges from a few meters to more than 10 m (Figures 2a, b).

The granite residual soil samples were collected from Minqing County, Fujian Province, a region historically affected by typhoon-induced landslides. Sampling followed the Chinese National Standard for Geotechnical Testing (GB/T 50123-2019) to ensure consistency. Three intact soil profiles were excavated at depths of 1.5–2.5 m within landslide-prone slopes, avoiding surface vegetation and weathered crusts. A total of 36 undisturbed cylindrical samples (diameter 50 mm, height 100 mm) were extracted using a thin-walled Shelby tube sampler to minimize disturbance. To account for profile heterogeneity, samples were collected from three distinct stratigraphic layers (upper, middle, lower) within each profile, with 12 replicates per layer.

The pertinent physical property test results for the soil samples are displayed in Table 1. The XRD diffraction test reveals that, aside from a significant presence of quartz in the soil's mineral composition, the parent rock has undergone substantial weathering, resulting in the predominance of kaolinite and illite,

with a minor amount of chlorite also present. The granular gradation curve of granite residual soil was obtained through a screening test (Figure 2c). It reveals that the proportion of granular groups with a particle size less than 2 mm exceeds 95%, while the content of fine-grained components less than 0.075 mm is less than 10%. The dominant particle size is concentrated in the range of 0.5–2 mm, indicating poor gradation, and the soil is classified as residual clay.

2.2 Testing scheme

The sample takes into account the state changes of granite residual soil throughout the entire process of unsaturation-saturation-persistent saturation in the actual rainfall environment. Two test conditions are used to characterize the unsaturation-saturation and persistent saturation stages of the soil sample (Table 2).

Direct shear test can better simulate the progressive failure process that may occur in actual slopes, and this failure process is often accompanied by strain localization, that is, concentrated deformation and failure occur in a specific area (Hanna and Ayadat, 2021). Therefore, direct shear test has unique advantages in studying the shear strength characteristics of slope materials.

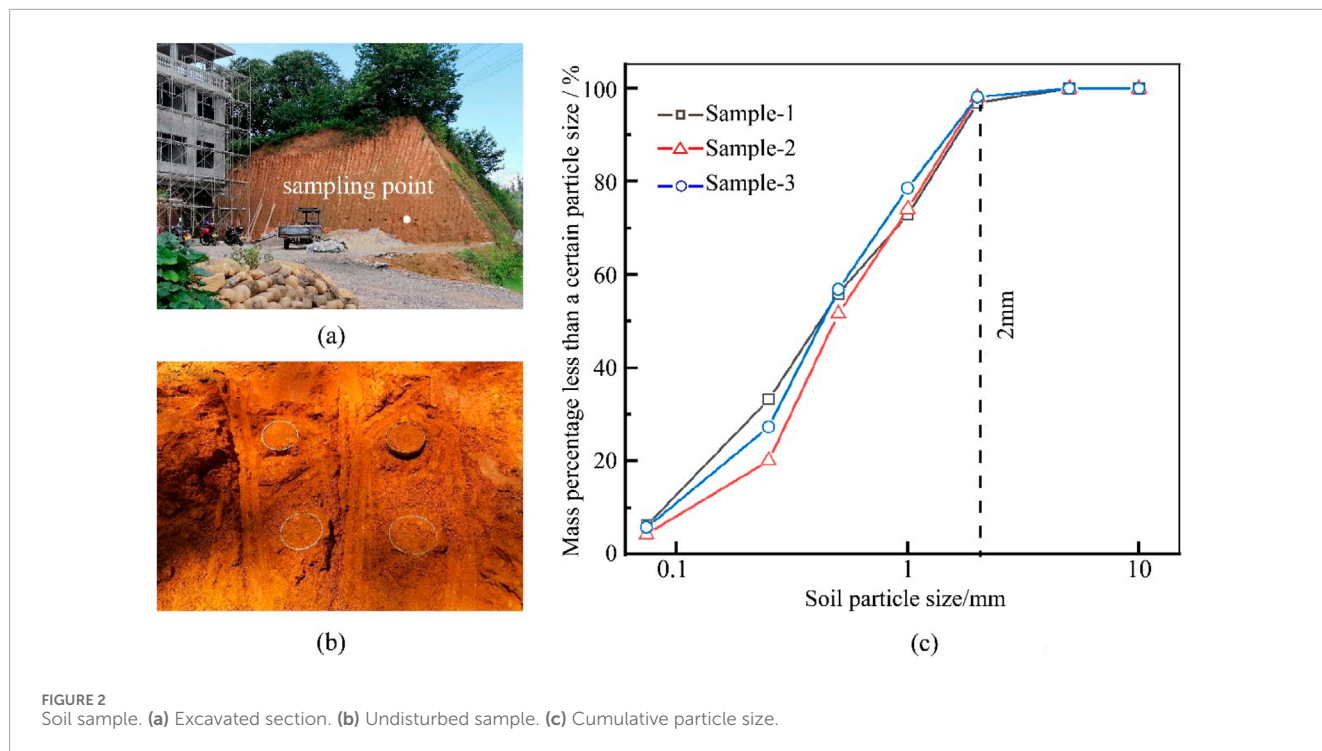


TABLE 1 Basic physical parameters of granite residual soil.

Dry density (g/cm ³)	Natural moisture content (%)	Saturated moisture content (%)	Liquid limit (%)	Plastic limit (%)	Mineral content (%)			
					Quartz	Kaolinite	Illite	Chlorite
1.30	24.26	30.00	40.56	26.42	33	52	12	3

TABLE 2 Testing scheme.

Test condition	Layer					
Moisture content (%)	10	15	20	22	25	30
Saturated time (h)	3	6	12	24	48	72

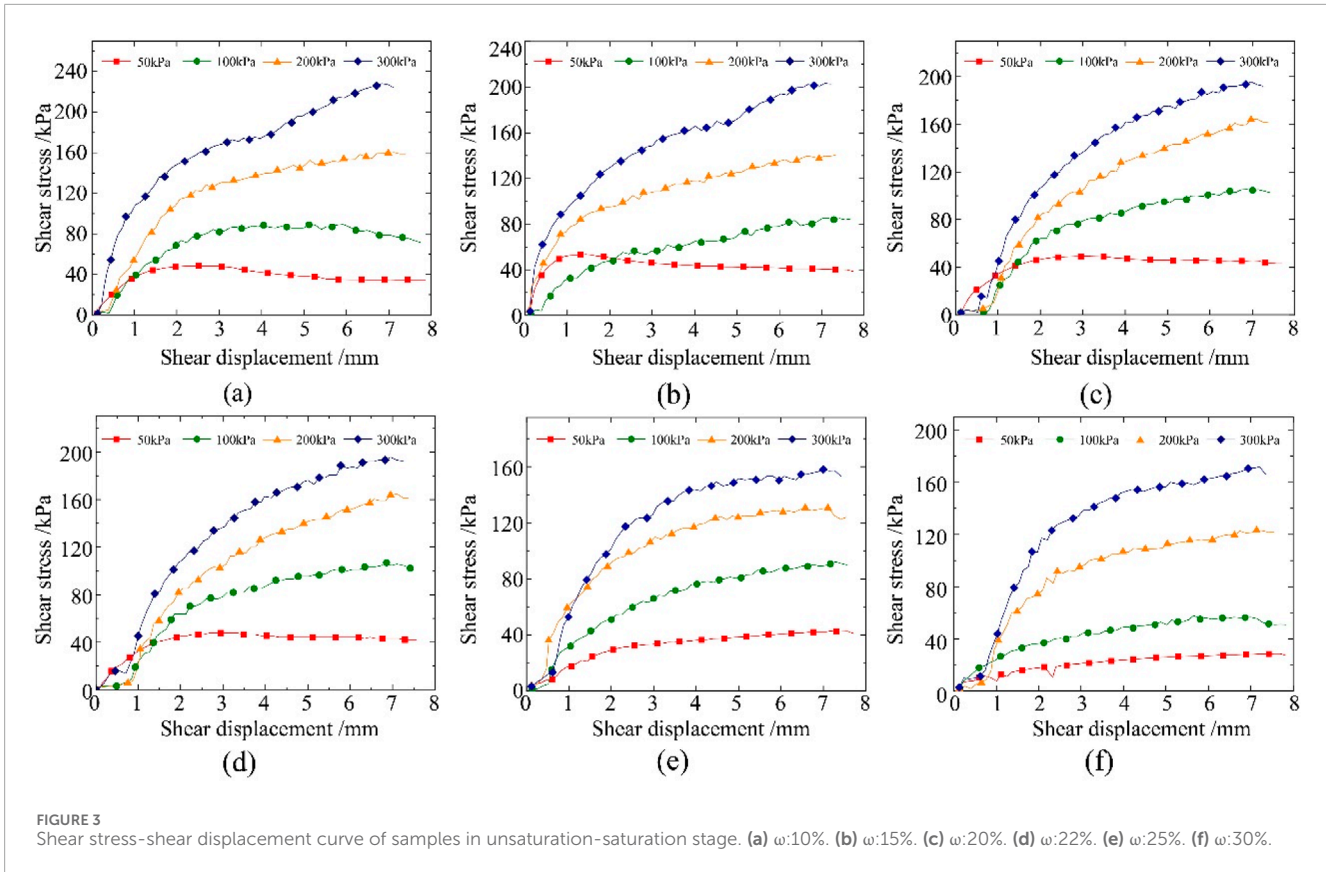
The test instrument adopts DJY-4L quadruple equal strain direct shear instrument, and the shear rate is 0.8 mm/min. After sieving, the dried granules less than 2 mm were remodeled, the dry density of the sample was 1.3 g/cm³, and the moisture content of the saturated mass was 30%. According to the test conditions, the initial moisture content samples were weighed and prepared according to the mass moisture content. The selected normal stress gradient (50 kPa, 100 kPa, 200 kPa, and 300 kPa) was determined to systematically cover the soil's natural stress state at the sampling depth (1.5 m, ~27–30 kPa) and to investigate its mechanical behavior under progressively increasing compressive stresses, including particle rearrangement and shear-induced failure mechanisms. After the direct shear test was completed, the shear samples were selected

for static electron microscope scanning test. Using a Thermo-Fisher scanning electron microscope (model Prisma E), images of the microstructure characteristics of the granite residual soil were obtained.

3 Strength characteristics in saturation process

3.1 Unsaturation-saturation stage

According to the direct shear test, the shear stress-shear displacement relationship curve of each moisture content layer sample was obtained (Figure 3), and then the shear strength change of the soil in the unsaturation-saturation stage was explored. According to the change range and development trend of the curve, the characteristics of the curve can be divided into two categories: weak strain softening type and strain hardening type. The weak strain softening curve demonstrates that the peak shear stress occurs during the shearing process. However, after the peak value, the shear stress drop is relatively small, and the rate of decrease is slow. This phenomenon is opposite to strain hardening, as under certain normal stress conditions, an increase in strain leads to a



reduction in the soil's shear strength. The phenomenon is mainly observed in samples with low moisture content and low normal stress conditions, such as $< 20\%$ and 50 kPa (i.e., the normal stress is 50 kPa, and the moisture content is less than 20%). At a moisture content of 22%, the curve characteristics shift towards strain hardening type. In this case, the shear stress increases with the shear displacement, and no peak shear stress is observed during the shear process. It can be divided into two categories based on the growth rate and amplitude of shear stress: weak strain hardening type and strong strain hardening type. The weak strain hardening type shows that the shear stress only increases slightly and slowly with the increase of the shear deformation, and tends to be stable after reaching a certain deformation. The curve features mainly appear in high moisture content and low normal stress environments, such as 25% and 50 kPa, 30% and 50 kPa, 30% and 100 kPa. The strong strain hardening type shows that with the increase of shear displacement, the shear stress increases significantly. This feature is particularly obvious in the environment of low moisture content and high normal stress, such as 10% and 300 kPa, 15% and 300 kPa, 20% and 300 kPa. Moreover, with the increase of moisture content, the curve characteristics are also changing. When the moisture content is low, the shear stress always maintains a strong growth trend until the sample is damaged; when the moisture content is high, the shear stress will increase significantly in the initial stage, but when the shear displacement reaches about 2 mm, the growth rate of the shear stress slows down significantly, and it shows a trend of stable development, and continuous shear deformation no longer requires more additional stress.

Quantitative analysis of shear stress evolution reveals distinct trends under varying moisture contents and normal stresses. For weak strain-softening samples (10% and 50 kPa), the peak shear stress drops by 12.7% (from 58.3 kPa to 51.2 kPa) after peak, with a stress reduction rate of 0.85 kPa/mm (calculated from post-peak slope). In contrast, strain-hardening samples under high normal stress (20% and 300 kPa) exhibit a shear stress increase rate of 2.1 kPa/mm, stabilizing at 245 kPa after 5 mm displacement. The transition from softening to hardening occurs at a critical moisture content of 18%, where the stress drop rate reduces to < 0.1 kPa/mm. The transition from weak to strong strain hardening is governed by pore water lubrication efficiency and structural degradation kinetics. Under low moisture content (10% and 50 kPa), limited pore water forms discrete liquid bridges between particles, inducing partial lubrication and weak hardening. As moisture increases ($> 20\%$), continuous water films reduce interparticle friction, while prolonged saturation (≥ 24 h) enhances pore water pressure dissipation, enabling stress redistribution through particle rearrangement. This dual mechanism—lubrication-driven friction reduction and viscous pore water energy dissipation—explains the accelerated hardening rates under high saturation.

Under the normal stress condition of 50 kPa, the shear failure characteristics of the sample are shown in Figure 4. During the state change of moisture content from low to high, the shear failure characteristics of the samples also showed obvious differences. At the low moisture content (Figure 4a), the specimen lacks sufficient pore water lubrication, leading to its breakage during the shear process. As a result, the integrity of the specimen after the shear is poor, and

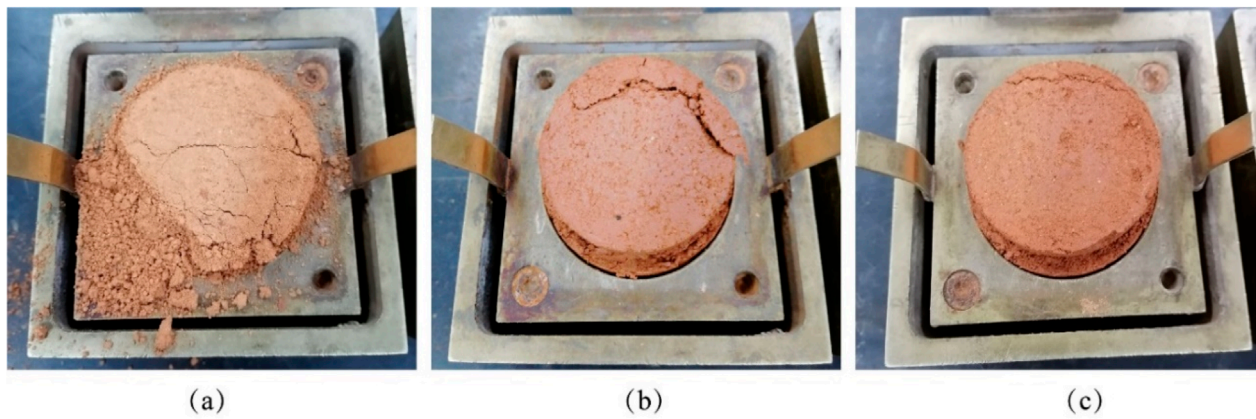


FIGURE 4 Failure characteristics of samples in unsaturation-saturation stage. (a) ω :15%. (b) ω :20%. (c) ω :25%.

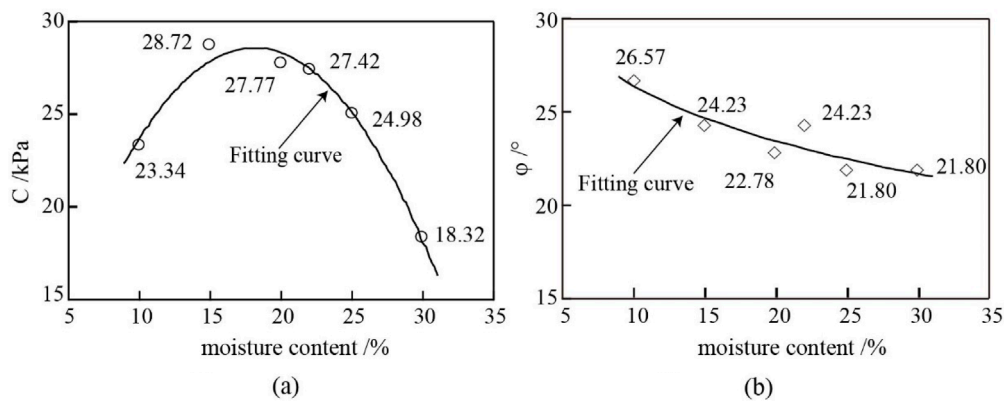


FIGURE 5 Relationship curve of shear strength parameter-moisture content. (a) C -moisture content. (b) φ -moisture content.

the friction characteristics of the shear surface become prominent. When the moisture content is high (Figures 4b, c), the integrity of the samples in the upper and lower sections of the shear plane is good, there is no obvious disintegration, the shear plane develops along the pushing direction, and the soil above and below the shear plane is not completely separated. Although shear failure occurs, it is not completely manifested as shear friction.

Based on the shear stress-shear displacement curve of the sample in the unsaturation-saturation stage, using Mohr-Coulomb theory, the relationship curve between cohesion (c) and internal friction angle (φ) and moisture content can be fitted and established (Figure 5).

With the increase of moisture content, the cohesion of granite residual soil increases firstly and then decreases, the peak value is near the 18% moisture content (Figure 5a), and the internal friction angle shows a continuous decreasing trend (Figure 5b). Through function fitting, in the unsaturation moisture content interval, the cohesion and moisture content have a quadratic function relationship, the degree of fitting (R^2) is 0.98 (Equation 1), the internal friction angle has a logarithmic function

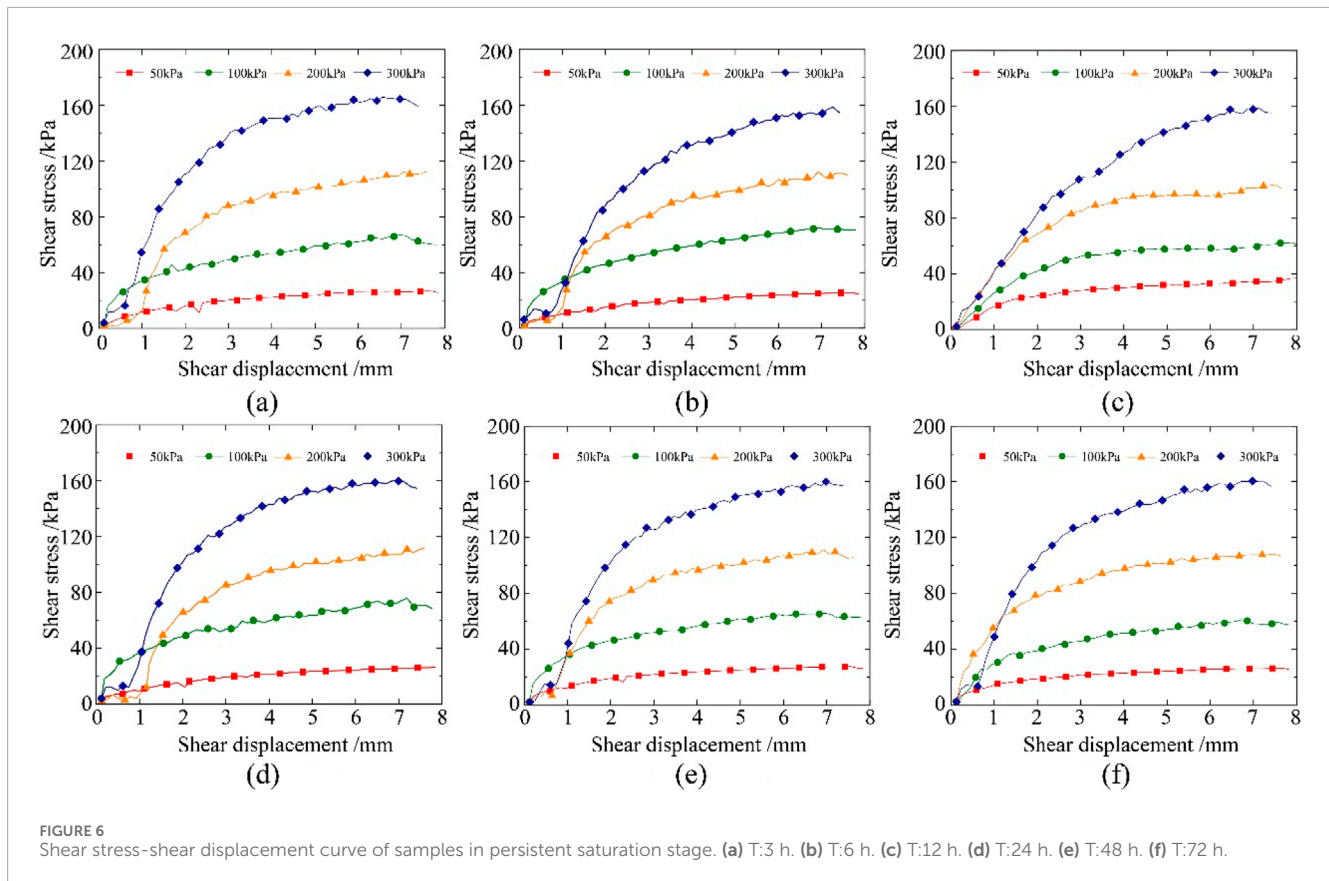
relationship with the moisture content, and the degree of fitting (R^2) is 0.85 (Equation 2).

$$C = -738.36\omega^2 + 267.75\omega + 4.29 \quad (1)$$

$$\varphi = -4.27 \ln \omega + 16.50 \quad (2)$$

where c —cohesion; φ —internal friction angle.

From the change range, the maximum and minimum values of cohesion are 28.7 kPa and 18.3 kPa, respectively, with a maximum decrease of 36.2%, while the internal friction angle continues to decrease with the increase of moisture content, but the overall change range is small, with a maximum decrease of 17.9%, it can be seen that the cohesion is affected by moisture content to a greater extent than the internal friction angle. At the rate of change, the cohesion decreases rapidly after reaching the peak value, while the internal friction angle decreases rapidly in the low moisture content range (<20%), and then the rate of change decreases and gradually stabilizes. In addition, Soil water content changes affect soil strength through altering its pore structure and water holding capacity. Beck-Broichsitter et al. (2023) found that gravel content impacts soil



porosity and pore structure, which affects water holding capacity and mechanical stability.

3.2 Continuous saturation state

Before the test, the sample was immersed in water for natural saturation treatment, so that the mass moisture content reached 30% (saturation state), and then the sample entered the persistent saturation stage. Under different saturation time conditions, the shear stress-shear displacement relationship curve of the sample is shown in Figure 6. Compared with the unsaturation stage, the curves of the samples in the persistent saturation state all show strain hardening type, but do not have the characteristics of strain softening type. Further analysis can still refine the curve characteristics into two types: weak strain hardening type and strong strain hardening type. The weak strain hardening type mainly appears in the low normal stress environment (50 kPa), but it also shows certain weak strain hardening characteristics when the saturation time is greater than 48 h and the normal stress reaches 100 kPa. Under the condition of higher normal stress, the specimen is more of a strong strain hardening type, and the shear stress required in the process of increasing shear deformation is also increasing, and this change is relatively significant. When the specimen reaches a certain deformation, the increase of shear stress gradually weakens and gradually stabilizes, and the overall change rate shows a development trend of gradually decreasing from large to large.

Under the normal stress condition of 50 kPa, the shear failure characteristics of the samples in the persistent saturation stage are shown in Figure 7. After natural immersion treatment, the samples showed overall deformation along the shear plane. After saturation, the viscosity of the soil is enhanced, and it no longer has the characteristics of dispersion and disintegration in the unsaturation state. With the increase of saturation time, the content of micro-pore gas decreases, and the water holding in the soil structure increases, resulting in the shear surface during the shear process. The free water nearby increased significantly, a large amount of pore water was discharged under the action of normal stress and shear stress, and the muddy phenomenon of the shear surface was also more significant. Due to the discharge of a large amount of pore water during the shearing process, coupled with the dislocation and displacement of the soil particles near the shearing surface, and even detachment from the original structure, it mixes with free water to form mud, which also has a lubricating effect on the shearing surface, resulting in prominent stick-slip characteristics of the soil after shearing.

Based on the shear stress-shear displacement curve of the sample in the persistent saturation stage, the relationship between cohesion (c) and internal friction angle (φ) and saturation time can be fitted and established by using Mohr-Coulomb theory (Figure 8).

We established a logarithmic function relationship between cohesion (c), internal friction angle (φ) and saturation time (T) through fitting analysis of the strength parameters of the granite

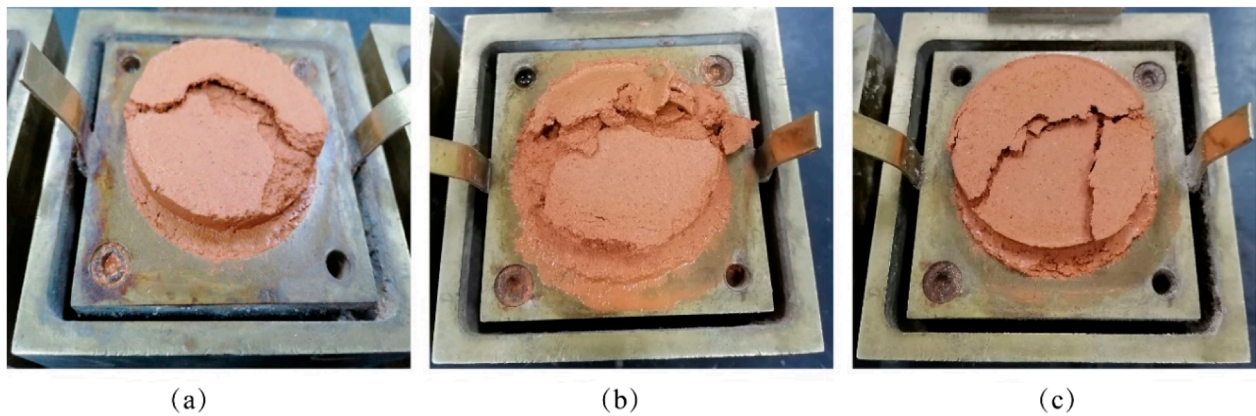


FIGURE 7 Failure characteristics of samples in persistent saturation stage. (a) T:3 h. (b) T:48 h. (c) T:72 h.

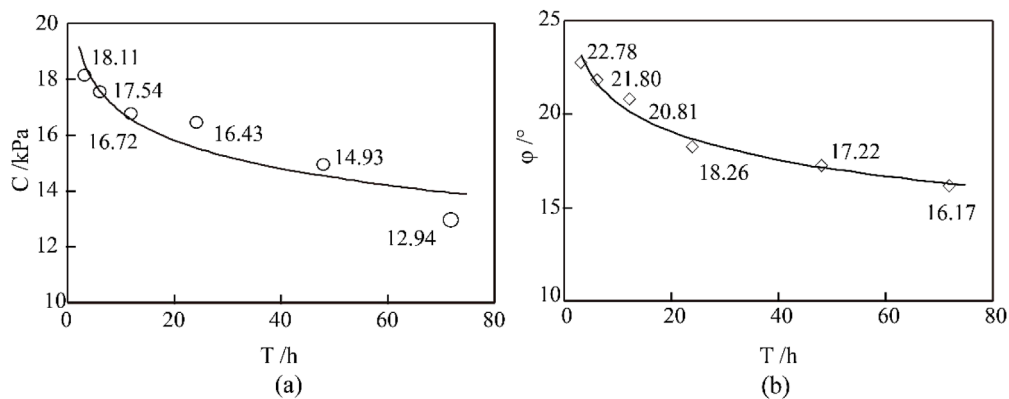


FIGURE 8 Relationship curve of shear strength parameter-saturation time. (a) C-T. (b) φ-T.

residual soil. Equations 3, 4 represent the relationship between the strength parameters of the granite residual soil and the saturation time, with degrees of fitting (R^2) of 0.88 and 0.98, respectively.

$$C = -1.45 \ln T + 20.15 \quad (3)$$

$$\varphi = -2.16 \ln T + 25.51 \quad (4)$$

where c —cohesion; φ —internal friction angle; T —time.

In the persistent saturation state, the cohesion and internal friction angle follow a similar decay pattern with the prolongation of saturation time, exhibiting a continuous decrease. Additionally, the rate of change also decreases over time, indicating a stable development trend. In addition, Ahmad et al. (2021), Ahmad et al. (2025) highlight that thermal cycles alter soil moisture distribution under dry-wet conditions, weakening structural stability in regions with significant temperature fluctuations. Concurrently, Nikolić et al. (2018) demonstrate that mesoscopic lattice unit models effectively simulate failure processes in heterogeneous materials, including crack propagation dynamics.

3.3 Mesoscopic structure characteristics and mechanism

The direct shear test provided the basis for selecting shear samples subjected to a normal stress of 50 kPa under various conditions. These samples were then subjected to static electron microscope scanning analysis to observe the change characteristics of their meso-structure. This analysis provides valuable evidence for understanding the intrinsic mechanism of water strength change.

3.3.1 Mesoscopic structure characteristics

3.3.1.1 Unsaturation-saturation stage

The meso-structure of the sample exhibits changing characteristics with an increase in moisture content, as illustrated in Figure 7. At the low moisture content, fine particles within the soil structure fill the gaps between coarse particle skeletons, leading to the formation of dense small pore groups comprising fine particle components (Figure 9a). The insufficient presence of lubricating and softening pore water hinders the displacement and rearrangement of particles during the shearing process, resulting in direct shear stress acting on the particle skeleton. The image obtained from

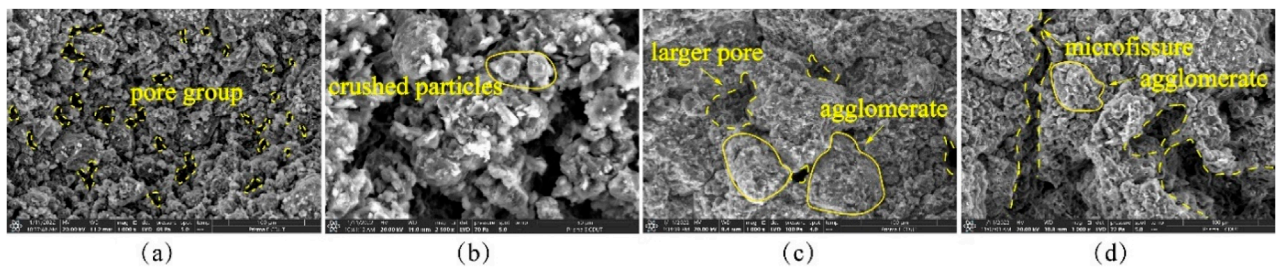


FIGURE 9
SEM images of microstructure of samples in unsaturation-saturation stage. (a) ω :10% (x1,000). (b) ω :10% (x2,500). (c) ω :15% (x1,000). (d) ω :30% (x1,000).

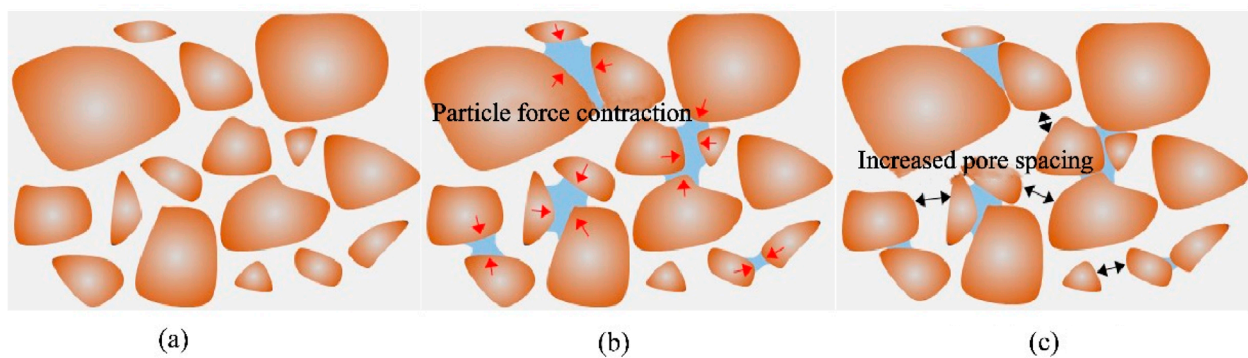


FIGURE 10
Schematic diagram of the effect of pore water on structure. (a) Primitive pore structure. (b) Particles aggregation. (c) Particle separation.

the 2,500 times viewing angle clearly shows particles undergoing shear and breaking as a result of stress concentration (Figure 9b). Consequently, the sample exhibits more brittle characteristics, resulting in a fully penetrating shear failure section and poor soil integrity. During the initial phase of moisture content growth, pore water creates a concave liquid surface due to matrix suction, leading to the shrinkage and convergence of adjacent soil particles (Figures 10a, b). Subsequently, these particles form agglomerates (Figure 9c) interconnected by pore water. The soil cohesion increases and reaches a peak at 18% moisture content. Meanwhile, particles adjacent to the pore gas become separated (Figure 10c), leading to the fusion and connection of small pores, thereby forming larger-sized pore structures and even evolving into micro-cracks (Figure 9d). As the moisture content significantly increases (above 18%), the matrix suction decreases, resulting in a reduction in pellet size (Figures 9c, d).

The meso-structural evolution directly governs the soil's macroscopic shear behavior through two interrelated mechanisms. First, clay-humic agglomerates—formed under low moisture conditions via capillary bonding—enhance inter-particle cohesion by creating stable microstructural frameworks (Figure 9c). These agglomerates increase the effective contact area between particles, elevating shear resistance until moisture exceeds 18%, at which point matrix suction diminishes and agglomerates disintegrate (Figure 9d). This collapse reduces cohesive bonds and weakens the soil's ability to resist shear deformation. Second,

pore structure reorganization plays a critical role: in unsaturated states, small pores dominate, promoting interlocking and high internal friction angles. As moisture increases, pore coalescence forms macropore, reducing intergranular friction and enabling strain-hardening behavior via lubricated particle sliding. Under prolonged saturation, pore water homogenizes the microstructure, lowering ϕ by 17.9% and stabilizing stress-strain responses. These transitions—from discrete agglomerates to dispersed particles and from heterogeneous to uniform pore networks—explain the nonlinear decay of cohesion and friction angle with moisture and saturation time.

3.3.1.2 Persistent saturation stage

The change characteristics of the sample meso-structure with the increase of saturation time are shown in Figure 11 at 500 times the viewing angle. Following saturation through immersion treatment, the proportion of pore water in the soil structure significantly increases. As the saturation duration prolongs, the development of the soil structure after shearing shows an opposite trend compared to the unsaturation state, wherein the pore size, number, and pellets exhibit an overall decrease. On one hand, the process of pore water filling progresses from easy to difficult as saturation time prolongs. The increased sufficiency of pore water filling leads to a reduction in the number and size of residual pores. Additionally, due to varying water holding capacities of pores, some disconnections or small pores exist in

the natural immersion state (Zhai et al., 2016). As a result, the soil structure gradually exhibits the development characteristics of False compaction. On the other hand, the reduction of agglomerates significantly contributes to the change in pore structure. During the unsaturation state, the main factor leading to agglomerate formation among soil particles is the matrix suction due to the difference between pore gas and pore water. However, as saturation time prolongs, the matrix suction approaches zero, resulting in a decrease in agglomerates within the structure during the flooding process. The mutual dispersion of soil particles leads to the cutting of large pores, primarily manifesting in the form of small pores in the soil structure. In addition, as an effective numerical method, the lattice unit model can better capture the initiation and propagation process of cracks in geotechnical materials in the microstructure than the traditional continuum mechanics method, and is particularly suitable for analyzing cemented geological materials with differences in porosity and composition (Rizvi et al., 2020).

3.3.2 Mechanism of strength reduce

The direct shear test results reveal that the mechanical strength of granite residual soil exhibits an overall decay trend under both test conditions, with intermittent increases observed only in the unsaturation state. The granite residual soil is abundant in secondary minerals, such as kaolinite and illite, which exhibit strong hydrophilicity. Scanning electron microscope images illustrate the changes in the soil structure. The decay of shear strength is attributed to the alterations in the meso-structure of the soil caused by water interactions. However, the impact of different conditions on the soil varies in terms of the mechanism of action.

3.3.2.1 Moisture content

The test conditions simulate the early stage of rainfall-induced state change in granite residual soil. During the initial growth of moisture content, the soil experiences significant matrix suction, leading to the formation of cohesive agglomerates among soil particles due to the influence of pore water tension. Excessive increase in moisture content leads to a weakening of matrix suction, reduced interaction among pore water particles, and subsequent decrease in cohesion. Throughout the entire process of moisture content growth, the frictional resistance between particles continuously decreases due to pore water lubrication. Cohesion plays a significant role in the shear strength index, leading to an initial increase and subsequent decrease in overall soil shear strength with rising moisture content.

3.3.2.2 Saturation time

Upon reaching saturation, the soil enters a persistent saturation stage. When the moisture content approaches saturation, the matrix suction significantly decreases, leading to partial decomposition of agglomerates and the division of large pores by particles. As the saturation time increases, the agglomerates formed in the early stage gradually vanish, resulting in reduced soil cohesion. Simultaneously, the pore water continues to fill the tiny pores in the structure, maximizing the natural water-holding effect of the granite residual soil. From a structural perspective, the cohesive force of the granite residual soil decreases due to granule disintegration, and the friction strength is further reduced by the increased prominence

of pore water lubrication, ultimately leading to the attenuation of the mechanical strength of the granite residual soil. Additionally, during the early stage of flooding, the soil-water interaction time is short, resulting in a relatively higher proportion of pore gas residues, thereby impacting the mechanical strength of the granite residual soil. As the saturation time is prolonged, the pore gas is gradually discharged, replaced by pore water, leading to an expanded range of soil-water mutual feedback. The mechanical strength of granite residual soil, under the comprehensive action, exhibits an initial rapid decrease followed by a gradual stabilization. In addition, the finite element method has been widely applied to assess geological stability, as shown by Alsbhan et al. (2021) in tunneling simulations. Meanwhile, recent multiphase models (Bai et al., 2023; Bai et al., 2025) integrate microscopic energy dissipation with nonlinear binding stress, multiphase dynamics, and thermal coupling, enhancing sediment behavior predictions across varying hydrate saturations and porosities.

4 Discussion

During a disaster event triggered by heavy rainfall, the initial response of the seepage field in the granite residual soil slope is driven by rainfall infiltration. As the seepage field evolves and develops, the soil and water engage in mutual feedback concurrently. Pore water action damages the soil structure, leading to a feedback effect on the soil's mechanical strength, ultimately influencing the macroscopic stability of the slope. The instability failure mechanism of granite residual soil, considering its unique physical and mechanical properties and the impact of rainfall-induced residual layer landslides, is categorized into four stages: original slope evolution, rainfall infiltration, creep-cracking-gradual failure, and slope erosion.

4.1 Primitive slope evolution stage

The granite residual soil in the area and the slope body exhibit special physical properties such as good permeability, gradation, and water strength attenuation due to the combined influence of climate, structure, and rock mass properties, resulting in a unified binary structure (Figure 12a).

4.2 Rainfall infiltration and saturation stages

During the initial rainfall stage, most of the rainwater infiltrates into the soil, with a small portion generating surface runoff. This marks the unsaturation-saturation development stage of the granite residual soil. During rainfall, the moisture content changes, resulting in the formation of a wet front on the shallow surface of the slope that progressively extends inward. Simultaneously, a stable and developing seepage field rapidly forms within the slope. As a result, rainfall not only infiltrates downward in the residual layer but also flows along the slope, creating a seepage force in that direction. The combined effect of gravity and seepage force results in uneven moisture content distribution, leading to the formation

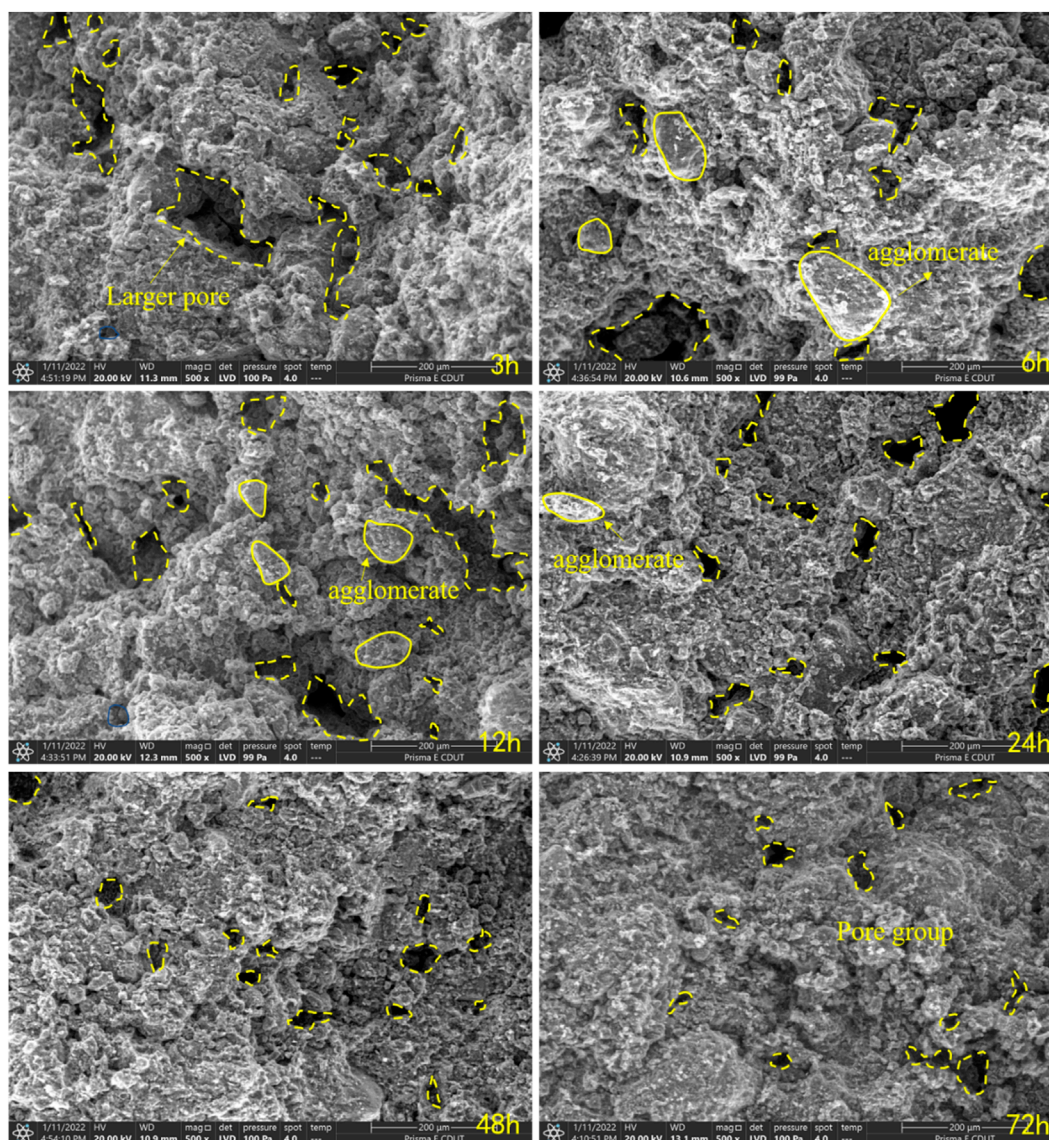


FIGURE 11
SEM images of microstructure of samples in persistent saturation stage.

of a saturated area at the foot of the slope. Consequently, the shear strength of the soil in this saturated region significantly decreases. Simultaneously, the soil in the middle and upper part of the slope experiences an early stage of moisture content increase, resulting in the formation of cohesive agglomerates that lead to a slight rise in its shear strength. Consequently, landslides typically initiate near the foot of the slope (Figure 12b).

It should be noted that, in this study, direct measurements of pore water pressure were not conducted. Pore water pressure is a critical factor influencing slope stability, particularly during rainfall events. The buildup of pore water pressure can reduce the effective stress within the soil matrix, thereby diminishing the shear strength of the soil. This process is closely related to the infiltration of rainwater and the development of seepage forces within the slope. Future research should consider incorporating direct pore water pressure monitoring to better understand its temporal and spatial

variations during rainfall, as well as to quantify its relationship with slope stability more accurately. Additionally, laboratory experiments could be designed to investigate the effects of pore water pressure under different soil conditions and rainfall scenarios, providing more comprehensive insights into the mechanisms of rainfall-induced slope failures.

4.3 Creep-crack-progressive failure stage

Continuously influenced by rainfall, the saturated area progressively extends towards the upper and deeper regions of the slope, resulting in the soil at the foot of the slope being in a persistent saturation stage. As the immersion time prolongs, the matrix suction diminishes, and the water-holding capacity of the pore structure reaches its peak. Consequently, the soil structure undergoes further

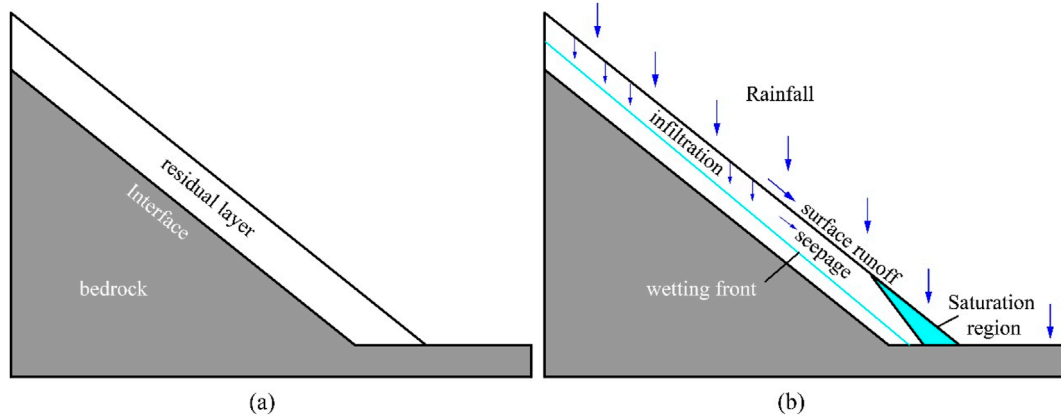


FIGURE 12 Primitive slope evolution. (a) Rainfall infiltration. (b) Saturation stages.

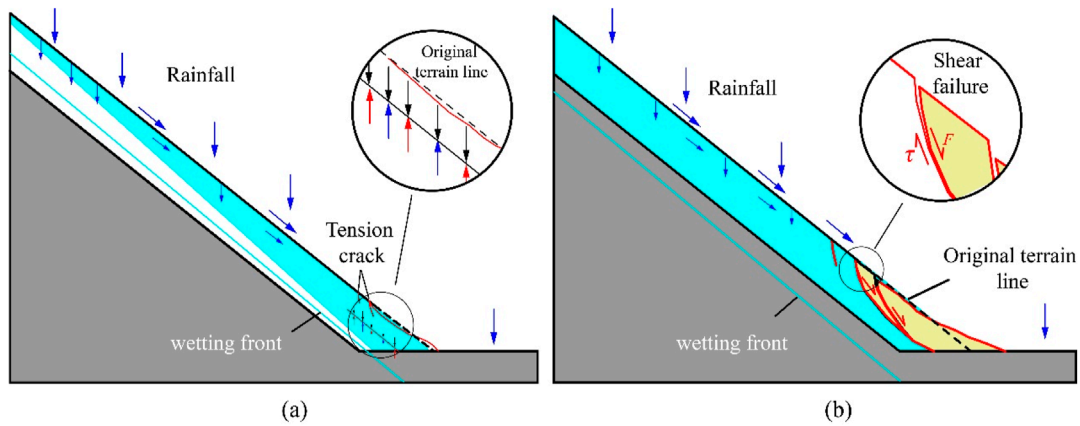


FIGURE 13 Creep-crack-progressive failure stage. (a) Slope creep and tensile cracking. (b) Progressive failure.

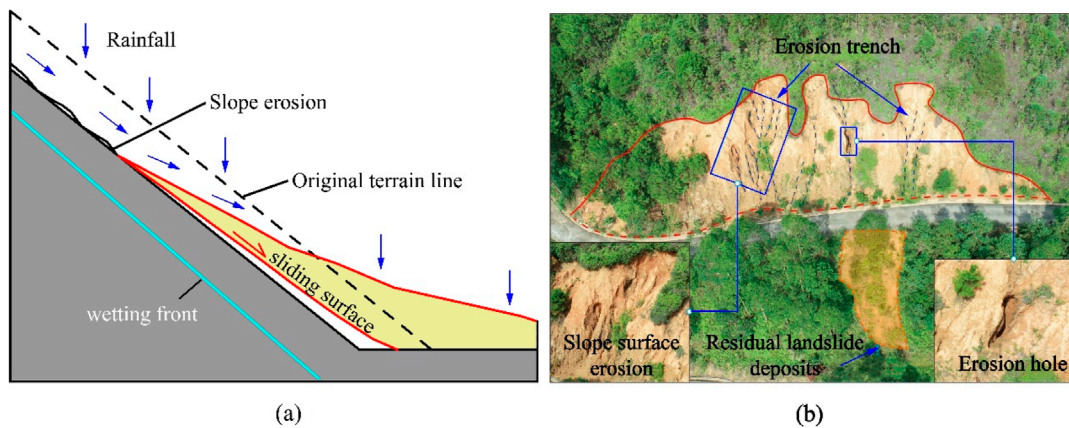


FIGURE 14 Slope erosion stage. (a) Slope erosion failure mode. (b) Post erosion characteristics.

damage, resulting in a continued decline in strength. By conducting force analysis, it is evident that continuous rainfall intensifies the soil's conditions within the persistent saturation region, leading to a considerable increase in the stress σ in the upper part of the soil. Additionally, due to the soil's excellent permeability, the rise in pore water pressure u is minimal, thereby placing the burden of stress on the soil particle skeleton. This leads to an increase in the value of σ' . Concurrently, the influence of the seepage force causes the soil to undergo slight deformation, displaying creep characteristics on the slope. Such deformation traits generally involve small variations and rapid developments, which can often pose challenges in practical cases. As the creep progresses, the deformation zone exhibits the emergence of tensile cracks (Figure 13a). Cracks facilitate the additional infiltration of rainwater. Consequently, the sliding force rises with the increased soil weight, leading to a further reduction in the soil's shear strength. As a result, local blocks near the foot of the slope, soaked for an extended duration, experience shear damage along the cracks. Following the damage, a new sliding plane forms, causing the upper sliding body to collapse and entering the gradual failure stage. The progressive failure extends until reaching the top of the slope, resulting in overall instability of the landslide (Figure 13b).

4.4 Slope erosion stage

Once the landslide becomes unstable, the sliding body covers the foot of the slope, creating anti-sliding resistance, while the deep seepage field environment reaches a state of equilibrium. Electron microscope scanning experiments reveal a significant reduction in soil pore size during this process. Consequently, a substantial portion of rainwater is unable to infiltrate and instead becomes surface water, leading to a continuous rise in surface runoff and increased erosion initiation on the slope (Figure 14a). Loose deposits are transported by water flow, displaying typical characteristics of flow-induced damage. This phenomenon results in soil erosion, silt accumulation on roads and houses near landslides, and a subsequent expansion of the disaster's impact zone. Rainfall runoff initiates erosion on the slope surface, leading to the formation of grooves or cavities. This erosion process recurs during every typhoon rainfall event, leading to a continual enlargement of the deformation and damage area (Figure 14b).

5 Conclusion

This paper explores the mechanical strength changes in granite residual soil across unsaturated, saturated, and persistently saturated states, revealing the underlying mechanisms through electron microscope scanning tests. As the soil transitions from unsaturated to saturated and finally to persistently saturated, its shear strength first rises then falls. The shear stress-shear displacement curve shows strain softening at low moisture content but strain hardening otherwise. During the unsaturation-saturation phase, cohesion initially increases then decreases, while the internal friction angle steadily declines, correlating quadratically and logarithmically with moisture content, respectively. The shear strength peaks at 18% moisture content. In the persistent saturation phase, both cohesion and internal friction angle decrease logarithmically with saturation

time, accompanied by pronounced stick-slip behavior post-shear. Heavy rainfall triggers a progressive strength decay in slope soil, starting from the foot and leading to overall sliding with erosion and fluidization. The landslide process can be divided into four stages: original slope evolution, rainfall infiltration and saturation, creep-cracking-gradual failure, and slope erosion.

Data availability statement

The original contributions presented in the study are included in the article/supplementary material, further inquiries can be directed to the corresponding author.

Author contributions

BL: Conceptualization, Investigation, Methodology, Writing – original draft. BJ: Investigation, Writing – original draft. YW: Conceptualization, Investigation, Writing – original draft. XY: Supervision, Writing – original draft, Writing – review and editing. WF: Funding acquisition, Investigation, Methodology, Writing – review and editing. YL: Visualization, Writing – review and editing.

Funding

The author(s) declare that financial support was received for the research and/or publication of this article. This research was funded by the National Natural Science Foundation of China (Grant No. U2005205) and the Opening Fund of Key Laboratory of Geohazard Prevention of Hilly Mountains. Ministry of Natural Resources (Fujian Key Laboratory of Geohazard Prevention) (FJKLGH2024K005).

Acknowledgments

The authors wish to thank all reviewers for their helpful comments and suggestions.

Conflict of interest

The authors declare that the research was conducted in the absence of any commercial or financial relationships that could be construed as a potential conflict of interest.

Generative AI statement

The authors declare that no Generative AI was used in the creation of this manuscript.

Publisher's note

All claims expressed in this article are solely those of the authors and do not necessarily represent those of their affiliated

organizations, or those of the publisher, the editors and the reviewers. Any product that may be evaluated in this article, or claim that may be made by its manufacturer, is not guaranteed or endorsed by the publisher.

References

- Ahmad, S., Rizvi, Z., Arp, J., Wuttke, F., Tirth, V., and Islam, S. (2021). Evolution of temperature field around underground power cable for static and cyclic heating. *Energies* 14 (23), 8191. doi:10.3390/en14238191
- Ahmad, S., Rizvi, Z. H., and Wuttke, F. (2025). Unveiling soil thermal behavior under ultra-high voltage power cable operations. *Sci. Rep.* 15 (1), 7315. doi:10.1038/s41598-025-91831-1
- Alsabhan, A. H., Sadique, M. R., Ahmad, S., Alam, S., and Binyahya, A. S. (2021). The effect of opening shapes on the stability of underground tunnels: a finite element analysis. *Geomate J.* 21 (87), 19–27. doi:10.21660/2021.87.j2267
- An, R., Kong, L. W., Li, C. S., and Luo, X. Q. (2020). Strength attenuation and microstructure damage of granite residual soils under hot and rainy weather. *Chin. J. Rock Mech. Eng.* 39, 1902–1911. doi:10.13722/j.cnki.jrme.2020.0073
- An, R., Kong, L. W., Zhang, X. W., Guo, A. G., and Bai, W. (2023). A multi-scale study on structure damage of granite residual soil under wetting-drying environments. *Chin. J. Rock Mech. Eng.* 42, 758–767. doi:10.13722/j.cnki.jrme.2022.0211
- Bai, B., Zhang, B., Chen, H., and Chen, P. (2025). A novel thermodynamic constitutive model of coarse-grained soils considering the particle breakage. *Transp. Geotech.* 50, 101462. doi:10.1016/j.trgeo.2024.101462
- Bai, B., Zhou, R., Yang, G., Zou, W., and Yuan, W. (2023). The constitutive behavior and dissociation effect of hydrate-bearing sediment within a granular thermodynamic framework. *Ocean. Eng.* 268, 113408. doi:10.1016/j.oceaneng.2022.113408
- Bai, H., Feng, W., Yi, X., Fang, H., Wu, Y., Deng, P., et al. (2021). Group-occurring landslides and debris flows caused by the continuous heavy rainfall in June 2019 in Mibei village, Longchuan county, Guangdong province, China. *Nat. Hazards* 108, 3181–3201. doi:10.1007/s11069-021-04819-1
- Bai, H., Feng, W., Li, S., Ye, L., Wu, Z., Hu, R., et al. (2022). Flow-slide characteristics and failure mechanism of shallow landslides in granite residual soil under heavy rainfall. *J. Mt. Sci.* 19, 1541–1557. doi:10.1007/s11629-022-7315-8
- Beck-Broichsitter, S., Rizvi, Z. H., Horn, R., and Wuttke, F. (2023). Effect of gravel content on soil water retention characteristics and thermal capacity of sandy and silty soils. *J. Hydrol. Hydromech.* 71 (1), 1–10. doi:10.2478/johh-2023-0001
- Cui, Z. J., Yang, J. Q., and Chen, Y. X. (2007). The type and evolution of the granite landforms in China. *Acta Geogr. Sin.* 62. doi:10.3321/j.issn:0375-5444.2007.07.001
- Feng, W., Bai, H., Lan, B., Wu, Y., Wu, Z., Yan, L., et al. (2022). Spatial-temporal distribution and failure mechanism of group-occurring landslides in Mibei village, Longchuan county, Guangdong, China. *Landslides* 19, 1957–1970. doi:10.1007/s10346-022-01904-9
- Gao, Q.-F., Jrad, M., Hattab, M., Fleureau, J. M., and Ameer, L. I. (2020). Pore morphology, porosity, and pore size distribution in kaolinitic remolded clays under triaxial loading. *Int. J. Geomech.* 20, 04020057. doi:10.1061/(ASCE)GM.1943-5622.0001682
- Griffiths, F. J., and Joshi, R. C. (1989). Change in pore size distribution due to consolidation of clays. *Géotechnique* 39, 159–167. doi:10.1680/geot.1989.39.1.159
- Hanna, A., and Ayadat, T. (2021). Comparative study of shear strength characteristics of dry cohesionless sands from triaxial, plane-strain and direct shear tests. *Geomech. Geoenviron.* 16 (2), 150–162. doi:10.1080/17486025.2019.1648882
- Hu, H., Hu, Z. P., and Ruan, R. (2020). Research on landslide simulated experiment and slope sliding mesoscopic rule of granite residual soil under heavy rainfall. *J. Xiamen Univ. Nat. Sci.* 59, 583–589. doi:10.6043/j.issn.0438-0479.201810023
- Huang, B., Qiu, M., Lin, J., Chen, J., Jiang, F., Wang, M. K., et al. (2019). Correlation between shear strength and soil physicochemical properties of different weathering profiles of the non-eroded and collapsing gully soils in southern China. *J. Soils Sediments* 19, 3832–3846. doi:10.1007/s11368-019-02313-7
- Li, C. S., An, R., Shu, R. J., and Kong, L. W. (2020b). Initial-disintegration analysis of granite residual soil and approximate simulation of mathematical morphology. *Chin. J. Rock Mech. Eng.* 39, 845–854. doi:10.13722/j.cnki.jrme.2019.0704
- Li, X., Liu, H., Pan, J., Li, D., and Wang, J. (2020a). Rainfall thresholds of shallow landslides in wuyuan county of jiangxi province, China. *Open Geosci.* 12, 821–831. doi:10.1515/geo-2020-0120
- Liu, W., Song, X., Huang, F., and Hu, L. (2019). Experimental study on the disintegration of granite residual soil under the combined influence of wetting-drying cycles and acid rain. *Geomat. Nat. Hazards Risk* 10, 1912–1927. doi:10.1080/19475705.2019.1651407
- Luo, X., Gao, H., He, P., and Liu, W. (2021). Experimental investigation of dry density, initial moisture content, and temperature for granite residual soil disintegration. *Arab. J. Geosci.* 14, 1060. doi:10.1007/s12517-021-07239-4
- Miao, F., Wu, Y., Torok, A., Li, L., and Xue, Y. (2022). Centrifugal model test on a riverine landslide in the three gorges reservoir induced by rainfall and water level fluctuation. *Geosci. Front.* 13, 101378. doi:10.1016/j.gsf.2022.101378
- Nikolić, M., Karavelić, E., Ibrahimbegovic, A., and Mišćević, P. (2018). Lattice element models and their peculiarities. *Arch. Comput. Methods Eng.* 25, 753–784. doi:10.1007/s11831-017-9210-y
- Pan, Y. L., Jian, W. X., Li, L. J., and Lin, Y. Q. (2020). A study on the rainfall infiltration of granite residual soil slope with an improved Green-Ampt model. *Rock Soil Mech.* 41, 2685–2692. doi:10.16285/j.rsm.2019.1734
- Rizvi, Z. H., Mustafa, S. H., Sattari, A. S., Ahmad, S., Furtner, P., and Wuttke, F. (2020). *Dynamic lattice element modelling of cemented geomaterials*. Springer, 655–665.
- Wang, H. B., Zhou, Y., Yu, G., Zhou, B., and Zhang, A. J. (2021). A triaxial test study on structural granite residual soil. *Rock Soil Mech.* 42, 991–1002. doi:10.16285/j.rsm.2019.2117
- Wei, X., Fan, W., Chai, X., Cao, Y., and Nan, Y. (2020). Field and numerical investigations on triggering mechanism in typical rainfall-induced shallow landslides: a case study in the ren river catchment, China. *Nat. Hazards* 103, 2145–2170. doi:10.1007/s11069-020-04075-9
- Wei, Y., Wu, X., Xia, J., Miller, G. A., Cai, C., Guo, Z., et al. (2019). The effect of water content on the shear strength characteristics of granitic soils in South China. *Soil Tillage Res.* 187, 50–59. doi:10.1016/j.still.2018.11.013
- Wu, C., and Lin, C. (2021). Spatiotemporal hotspots and decadal evolution of extreme rainfall-induced landslides: case studies in southern taiwan. *Water* 13, 2090. doi:10.3390/w13152090
- Xia, J., Zhang, L., Ge, P., Lu, X., Wei, Y., Cai, C., et al. (2022). Structure degradation induced by wetting and drying cycles for the hilly granitic soils in collapsing gully erosion areas. *Forests* 13, 1426. doi:10.3390/f13091426
- Yang, H., Yang, T., Zhang, S., Zhao, F., Hu, K., and Jiang, Y. (2020). Rainfall-induced landslides and debris flows in mengdong town, yunnan province, China. *Landslides* 17, 931–941. doi:10.1007/s10346-019-01336-y
- Yin, S., Huang, J., Li, X., Bai, L., and Zhang, X. (2022). Experimental study on deformation characteristics and pore characteristics variation of granite residual soil. *Sci. Rep.* 12, 12314. doi:10.1038/s41598-022-16672-8
- Zhai, Q., Rahardjo, H., and Satyanaga, A. (2016). Variability in unsaturated hydraulic properties of residual soil in Singapore. *Eng. Geol.* 209, 21–29. doi:10.1016/j.enggeo.2016.04.034
- Zhan, L., Zhang, Z., Chen, Y. M., Chen, R., Zhang, S., Liu, J., et al. (2018). The 2015 Shenzhen Catastrophic landslide in a construction waste dump: reconstitution of dump structure and failure mechanisms via geotechnical investigations. *Eng. Geol.* 238, 15–26. doi:10.1016/j.enggeo.2018.02.019
- Zhang, S., and Tang, H. M. (2013). Experimental study of disintegration mechanism for unsaturated granite residual soil. *Rock Soil Mech.* 34, 1668–1674. doi:10.16285/j.rsm.2013.06.009
- Zhang, X. W., Kong, L. W., Guo, A. G., and Tuo, Y. F. (2012). Evolution of microscopic pore of structured clay in compression process based on SEM and MIP test. *Chin. J. Rock Mech. Eng.* 31. doi:10.3969/j.issn.1000-6915.2012.02.021
- Zhao, Y. R., Yang, H., Huang, L., Chen, R., Chen, X., and Liu, S. (2019). Mechanical behavior of intact completely decomposed granite soils along multi-stage loading-unloading path. *Eng. Geol.* 260, 105242. doi:10.1016/j.enggeo.2019.105242
- Zhou, J. (2020). Preprocessing method of microstructure image of geotechnical materials. *Environ. Technol. Innovation* 19, 100924. doi:10.1016/j.eti.2020.100924